Environmental Science
Water Research & Technology

Mineralization of greywater organics by the ozone-UV advanced oxidation process: Kinetic modeling and efficiency

Journal:	*Environmental Science: Water Research & Technology*
Manuscript ID	EW-ART-07-2019-000653.R1
Article Type:	Paper
Date Submitted by the Author:	26-Aug-2019
Complete List of Authors:	Gassie, Lucien; University of Miami, Civil, Architectural, and Environmental Engineering Englehardt, James; University of Miami,

Optimization of the ozone-UV advanced oxidation process is complicated by competing reactions, and the evolution of pH and UV transmissivity during treatment. In this work the effect of these factors on TOC mineralization kinetics during nearly closed-loop greywater reuse was studied, and a model developed characterizing kinetics as a function of ozone and UV dose, expanding options for water reuse.

Mineralization of greywater organics by the ozone-UV advanced oxidation process: Kinetic modeling and efficiency

Lucien W. Gassie[a], James D. Englehardt[b]

[a]University of Miami. 1251 Memorial Drive, Coral Gables, FL 33146. l.gassie@umiami.edu

[b]University of Miami. 1251 Memorial Drive, Coral Gables, FL 33146. jenglehardt@miami.edu

Abstract

Ozone-UV advanced oxidation treatment can mineralize total organic carbon (TOC) in water without the addition of chemicals, representing an alternative to phase-transfer processes such as reverse osmosis for water reuse. However, efficiency is governed by competing principal reaction pathways, and limited information has been available for optimizing treatment in such applications. In this study a 1.2 m^3/day (320 GPD) pilot ozone-UV greywater reuse system was tested using simulated and real shower water, and resulting kinetic data were used to develop a kinetic model of TOC mineralization. H_2O_2 is produced by photolysis with ozone, and subsequent reactions produce hydroxyl radical, which mineralizes TOC. TOC mineralization efficiency is governed by TOC concentration (controlling transmissivity), pH throughout treatment, ozone-UV dose ratio, and the evolution of pH due to CO_2 production from TOC, which impacts oxidative efficiency dynamically. Modeled hydroxyl radical concentrations were ~10^{-10} M, as expected during water treatment and reuse, and the second order rate constant for reaction of hydroxyl radical with TOC was [1.7-7.6]*10^7 $M^{-1}s^{-1}$, similar to others reported for mineralization of wastewater organics. Minimum electrical energy for commercial UV and ozone equipment was assessed at 3.73 kWh/m^3/order of TOC mineralization, and modeling indicated a wide range of optimal dosing ratios. Treatment efficiency was found to depend strongly on a reactor design that ensures an influent TOC concentration low enough to allow effective transmission of UV radiation. Further development of the kinetic model to account dynamically for pH evolution as a function of TOC mineralization, reactor hydraulics, and mixing is recommended.

1. Introduction

Advanced wastewater treatment processes, particularly reverse osmosis (RO) and advanced oxidation processes (AOPs), are being studied and used to develop portable and stationary water reuse systems (1,2). RO transfers constituents to a concentrated phase, whereas AOPs generate hydroxyl radicals (•OH) to rapidly and indiscriminately oxidize organic matter, with capability to mineralize wastewater organics to carbon dioxide (3,4). Hence, limitations of RO-based reuse systems in these applications include management of the concentrate, as well as blending of the water/remineraliztion to as required to reduce corrosivity, and chemical addition as required for disinfection residual and membrane life extension (2,5–8). In contrast, AOP-based systems do not produce concentrate, and have been shown to avoid the formation of halogenated disinfection byproducts above potable water standards by mineralizing organics to below 0.5 mg/L total organic carbon (TOC), at competitive cost and energy demand (3,9–11). While energy usage can be low with an RO process, at ~0.5 kWh/m^3 (9), pretreatment, chemical addition, and concentrate disposal can significantly increase energy required, all of which depend on site and system conditions.

AOPs that have been applied for water reuse include UV-hydrogen peroxide (UV-H_2O_2), hydrogen peroxide-ozone (peroxone), UV-chlorine, and UV-titanium dioxide (4,6,12–16). However, these processes require transport of chemicals to the treatment site, making them less applicable in portable water reuse systems such as might be deployed militarily at a remote health care unit (10). In contrast, the ozone-UV process, while employing chemical mechanisms common to both the UV-H_2O_2 and peroxone processes, does not require chemical transport to the treatment site.

In the ozone-UV process, photolysis of ozone generates hydrogen peroxide, which then reacts with ozone as in the peroxone process, and with UV light as in the UV-H_2O_2 process (12). Thus, competing reactions between ozone, UV, hydrogen peroxide, hydroxyl radical, organics, and other radical scavengers, make process kinetics more complex than those of the peroxone and UV-H_2O_2 processes. In particular, pH and TOC concentration have strong effects on how much H_2O_2 can be formed by photolysis of ozone, and whether peroxone or UV-H_2O_2 reactions dominate (17,18). This is due to pH control of aqueous vs. ionized H_2O_2 in solution (influencing peroxone vs. UV-H_2O_2 reactions), and TOC blocking UV light, which limits both ozone photolysis and UV-H_2O_2 reactions.

Partly as a result of the competition just described, the ratio of ozone dose to UV fluence required to maximize oxidative degradation depends strongly on the water matrix. Also, for a particular UV reactor, increasing ozone dose will eventually yield diminishing returns in treatment efficiency, as competition of organics with ozone and hydrogen peroxide for hydroxyl radical becomes more important (18). However, little guidance was found regarding optimization of the ozone-UV dose (12,13,17–22). Further, while decentralized nonpotable greywater reuse has been well-reported (23–26), literature found on potable greywater reuse was limited to a study documenting human health risk of organic micropollutants in greywater (27).

The objectives of this paper are to characterize the chemical kinetics of the ozone-UV process in greywater reuse applications, and provide a working model of the mineralization of bulk organics measured as total organic carbon. Hence, a pilot ozone-UV treatment system, part of a net-zero greywater (i.e., nearly closed-loop) reuse system, was designed, constructed, and tested for compliance with the California direct potable reuse (DPR) framework goal of 0.5 mg/L maximum total organic carbon in the product water (2). Other DPR framework goals are

evaluated in a separate study (28). Synthetic and actual shower water was recycled at an 85% recycle rate with 15% RO-treated municipal water makeup, and analyzed at various stages of treatment for TOC, dissolved ozone, hydrogen peroxide, turbidity, alkalinity, electrical conductivity (EC), and pH. The model developed provides predicted TOC, a critical parameter for water reuse with human contact (2), along with concentrations of ozone, hydroxyl radical, and hydrogen peroxide in the water during treatment.

2. Materials and methods

2.1 System description

The pilot system includes two tanks, with shower water drawn from a treated water tank and drained to a greywater tank for subsequent treatment. The treated and greywater water tanks have working volumes of 0-300 L and 230-530 L (0-80 gallons and 60-140 gallons), respectively, both with ozone gas venting. Initial and makeup water were obtained by RO treatment of tap water using a 2-stage 0.8 m^3/day (200 GPD) domestic RO unit (StealthRO200, Hydrologic Purification Systems, CA, USA). The greywater tank is continuously circulated through the ozone-UV treatment system at a flow rate of 110 liters per minute (30 GPM), which consists of a 16-mesh strainer (McMaster-Carr, Elmhurst, IL), venturi ozone injection at a delivered rate of 25 g/hr (Maximum gas production capacity of 60 g/hr and transfer efficiency of 93% under experimental conditions), three parallel UV reactors with total output of 596 W and reflective walls designed to ensure that all UV light is absorbed (SPARTOX 60, Spartan Environmental Technologies, OH, USA; Neotech D338 and D438, Neotech Aqua Solutions, San Diego, CA, USA), and final 5-micron filter (Graver Stratum, Graver Technologies, Glasgow, DE, USA). The delivered 25 mg/L ozone dose corresponded to a concentration of 3.82 mg/L dissolved ozone in the UV reactor. The system continues to treat until TOC is <0.5 mg/L, which also ensures that

104 the water is disinfected (28), after which the treated water from the greywater tank discharges to
105 the treated tank for use. A system schematic is shown in Figure 1.

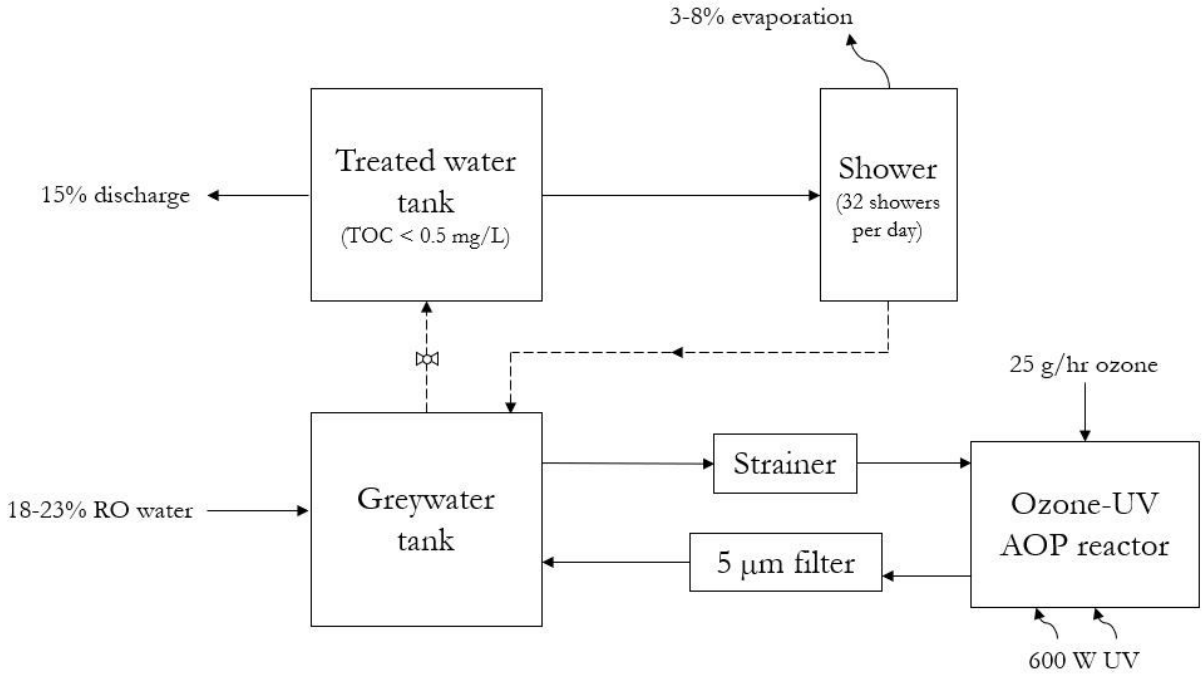

106
107 Figure 1. Schematic of the shower reuse system.

108 The system was designed to operate at 32 showers/day (1.2 m^3/day, 320 GPD). The
109 average TOC and UV_{254} of the greywater prior to dilution into the system were 56.47 mg/L and
110 0.229 cm^{-1}, respectively. To prevent buildup of excess minerals in the product water, 15% of the
111 water was discharged daily (45 liters per day/12 GPD during experiment days of 8 showers/day).
112 Afterwards, makeup water was added daily from the RO unit equal to the evaporation (3-8% of
113 daily flow, depending on weather, or 9.1-24 liters/2.4-6.4 gal) plus the discharge (45 liters/12 gal),
114 to prevent water loss. Evaporation was measured using an in-tank level sensor and tank
115 dimensions. In this work RO-treated tap water was used for makeup, though collected rainwater
116 might also be used. Full system details, including other water quality parameters, are reported in a
117 separate study (28). This project did not involve collecting data on human subjects, i.e. did not
118 involve collecting data containing any of the 18 specific identifiers noted in the privacy Rule (USA,

45 CFR 46); nevertheless, informed consent was obtained from human subjects taking showers in the system.

2.2 Materials

The soap and shampoo used in the showers was 25% Campsuds (Sierra Dawn Products, Graton, CA, USA) mixed with 0.635 M soda ash (simulated runs without conditioner) or 0.747 M soda ash (all other runs), diluted with deionized water to maintain low TOC and circumneutral pH in the greywater. This formulation was chosen to provide low COD and neutral pH, so as to maximize the rate of mineralization of organic impurities by the advanced oxidation process. The conditioner used was Garnier Fructis® Biodegradable Conditioner (L'Oréal S. A., Clichy, Hauts-de-Seine), and soybean oil was used to simulate body organics. Selection of these products is explained in detail elsewhere (28). All reagents were analytical grade and used as received.

2.3 Analytical Methods

TOC was measured by Hach method 10129 (Hach Company, Loveland, CO, USA) with a Beckman Coulter DU720 UV-Vis Spectrophotometer (Beckman Coulter, Inc, Brea, CA, USA). The detection limit for this test was assessed at 0.35 ± 0.03 mg/L. Hydrogen peroxide was measured by iodometric titration (29). pH and conductivity were measured using an Orion Star A3295 probe unit (Thermo Scientific, MA, USA), and turbidity was measured by nephelometer (Monitek Nephelometer TA1, Galvanic Applied Sciences, Inc., Calgary, Canada). Dissolved ozone was monitored with a sensor in the tank (ATI Q46H/64 Dissolved ozone monitor, ATI, Inc., PA, USA). Alkalinity was measured using Standard Method 2320 (30). Modeling was performed in Matlab Simulink 2017a (MathWorks, Inc., MA, USA). A linear calibration curve was established for TOC and tested with standard solutions once per month for accuracy.

2.4 Experiments

Two types of kinetic experiments were conducted. First, batch treatment of simulated shower water was tested in the greywater tank. For these runs, simulated shower water was added directly to the greywater tank, operating at a volume of 380 L (100 gallons), and samples were taken every 10 minutes to analyze for pH, TOC, and hydrogen peroxide concentration. The first experiment (Run 1) consisted of adding 52.5 g of the Campsuds solution, and 4.5 g of the soybean oil, or approximately three showers worth of soap and body organics, not including conditioner (10). It was then decided that in-shower conditioner would be necessary for users, in spite of its significant contribution to the turbidity, UV absorbance, and TDS of the water in laboratory tests (28). Hence, the second experiment (Run 2) involved addition of 35 g of the Campsuds solution, 3 g of soybean oil, and 7 g of conditioner, equivalent to approximately two showers. Each set was repeated in triplicate.

The second type of kinetic test involved treating actual shower water in the greywater tank, with no inflow or outflow. To simulate an efficient pilot design in which treatment begins during showering and continues thereafter in batch mode, treatment was started at the beginning of an initial two-hour period during which water from eight consecutive showers (taken every 15 minutes, 10 minutes per shower at (3.8 LPM [1.0 GPM] showerhead flow) drained directly to the greywater tank, which held an initial charge of 230 L (60 gal) of water that had been fully-treated previously and which then filled to a 530 L (140 gal) volume. Beginning at the end of this two-hour period, samples were taken every 15-30 minutes to analyze pH, TOC, and hydrogen peroxide, as treatment continued. Men used 10 g Campsuds solution and 1.23 g of conditioner, while women used 25 g of Campsuds solution and 4.93 g of conditioner, with equal number of men and women for each of the shower runs. For comparison, these experiments were run both

with (Run 3) and without (Run 4) a point-of-use GAC filter installed on the showerhead as a polishing step to remove potential organic and inorganic contaminants including bromate and nitrate that can accumulate in AOP-based water reuse systems (31,32). Three replicates of each run type were completed. Results are shown with error bars representing one standard deviation to represent the large variation in TOC observed across runs, attributed to variation in the cleanliness of subjects prior to showers. Results with and without GAC were modeled separately. Experimental conditions are summarized in Table 1.

Table 1. Summary of experiments conducted

Experiment	Greywater matrix	Relevant experimental conditions
Run 1	Simulated shower water (3 showers)	No conditioner
Run 2	Simulated shower water (2 showers)	With conditioner
Run 3	Actual shower water (8 showers, pretreated for two hours during shower period)	GAC filter prior to final sample
Run 4	Actual shower water (8 showers, pretreated for two hours during shower period)	No GAC filter prior to final sample

2.5 Modeling

The basis of the ozone-UV process is photolysis of ozone, shown in equation 1, which produces hydrogen peroxide, with a quantum yield of 0.62 (33).

$$O_3 + H_2O \xrightarrow{h\nu} O_2 + H_2O_2 \quad \textbf{(1)}$$

The production of hydrogen peroxide and the photolysis of ozone can be expressed by the following equations (13,34):

$$\frac{d[O_3]}{dt} = -\Phi_{O_3} P_{UV} f_{O_3} (1 - \exp(-2.3A)) \quad \textbf{(2)}$$

$$\frac{d[H_2O_2]}{dt} = \Phi_{O_3} P_{UV} f_{O_3} (1 - \exp(-2.3A)) \quad \textbf{(3)}$$

in which Φ_{O_3} is the quantum yield of ozone (0.64), P_{UV} is the intensity of the UV reactor per unit volume in einsteins/L-s (12), f_{O_3} is the fraction of UV light absorbed by ozone (35), and A is the total absorbance of the solution, given by Equation 6:

$$P_{UV} = \frac{P\eta}{N_{AV}Vh\nu} \quad \textbf{(4)}$$

$$f_x = \frac{[x]\varepsilon_x}{[O_3]\varepsilon_{O_3} + [H_2O_2]\varepsilon_{H_2O_2} + [TOC]\varepsilon_{TOC}} \quad \textbf{(5)}$$

$$A = b(\varepsilon_{O_3}[O_3] + \varepsilon_{H_2O_2}[H_2O_2] + \varepsilon_{TOC}[TOC]) \quad \textbf{(6)}$$

where P is the total reactor power in W, η is the reactor efficiency, set at an average of 19% as tested by intensity measurements in treated water at the reactor wall sensors (and as is within the manufacturer's claimed efficiency), N_{AV} is the Avogadro constant ($6.23*10^{23}$), V is reactor volume in L, h is Planck's constant ($6.62*10^{-34}$ J-s), and ν is the frequency of UV light, $1.18*10^{15}$ s^{-1} at 254 nm. In equation 5, x indicates either ozone, hydrogen peroxide, or TOC, in mol/L, while ε values are extinction coefficients for each compound, with $\varepsilon_{O_3} = 3300M^{-1}cm^{-1}$, $\varepsilon_{H_2O_2} = 17.9M^{-1}cm^{-1}$, and ε_{TOC} calculated during the model fitting process, based on measured TOC concentration and UV_{254} absorbance of water samples during treatment and using Equation 6 after subtracting absorbance due to measured hydrogen peroxide and TOC. Dissolved ozone was modeled to have decayed to negligible levels in the context of UV_{254} absorbance by the time the samples from the treatment tank were analyzed for the other parameters. *b* is the effective light path of the reactor in cm considering reactor internal reflection and retention of radiation.

Once ozone, hydrogen peroxide, and UV light are present in the water, hydroxyl radical formation occurs through two primary pathways. One of these is the photolysis of hydrogen peroxide, given by chemical equation 7 and rate equation 8 (35):

$$H_2O_2 \xrightarrow{h\nu} 2\,^{\bullet}OH \quad \textbf{(7)}$$

$$\frac{d[H_2O_2]}{dt} = -\Phi_{H_2O_2} P_{UV} f_{H_2O_2} (1 - \exp(-2.3A)) \quad \textbf{(8)}$$

The second reaction pathway involves the peroxone process, comprising a series of chain reactions leading to the net reaction shown in equation 9 (18):

$$2O_3 + H_2O_2 \xrightarrow{k_n} 2\,^{\bullet}OH + 3O_2 \quad \textbf{(9)}$$

in which k_n is the semi-empirical net rate constant for generation of hydroxyl radical in the peroxone reactions. The peroxone reactions are initiated by the conjugate base of hydrogen peroxide, with a pK of 11.8 (22):

$$H_2O_2 \overset{pK}{\leftrightarrow} HO_2^- + H^+ \quad \textbf{(10)}$$

Other key reactions in the ozone-UV process are given by equations 11-18 (13,18,22,35):

$$O_3 + OH^- \xrightarrow{k_{O_3,OH^-}} HO_2^- + O_2 \; (high\; pH) \quad \textbf{(11)}$$

$$3O_3 + OH^- \xrightarrow{k_{n1}} 2\,^{\bullet}OH + 4O_2 \; (net\; reaction,\; high\; pH) \quad \textbf{(12)}$$

$$O_3 + HO_2^- \xrightarrow{k_{O_3,\,H_2O_2}} O_3^- + {}^{\bullet}HO_2^- \quad \textbf{(13)}$$

$${}^{\bullet}HO_2^- \overset{pK_2}{\leftrightarrow} {}^{\bullet}O_2^- + H^+ \quad \textbf{(14)}$$

$$O_3 + {}^{\bullet}O_2^- \xrightarrow{k_{O_3,{}^{\bullet}O_2^-}} {}^{\bullet}O_3^- + O_2 \quad \textbf{(15)}$$

$$O_3 + {}^{\bullet}OH \xrightarrow{k_{O_3,{}^{\bullet}OH}} {}^{\bullet}HO_2 + O_2 \quad \textbf{(16)}$$

$$H_2O_2 + {}^{\bullet}OH \xrightarrow{k_{H_2O_2,{}^{\bullet}OH}} {}^{\bullet}HO_2 + H_2O \quad \textbf{(17)}$$

$$HCO_3^- + {}^{\bullet}OH \xrightarrow{k_{HCO_3^-,{}^{\bullet}OH}} H_2O + {}^{\bullet}CO_3^- \quad \textbf{(18)}$$

Oxidation of TOC by (a) direct UV photolysis and (b) direct oxidation by ozone (equations 19 and 20) was also evaluated to determine if these pathways were significant relative to hydroxyl radical oxidation in the greywater organic matrix:

$$\frac{d[TOC]_{UV}}{dt} = -\Phi_{TOC} P_{UV} f_{TOC} (1 - \exp(-2.3A)) \quad \textbf{(19)}$$

$$\frac{d[TOC]_{O_3}}{dt} = -k_{O_3,TOC}[O_3][TOC] \quad \textbf{(20)}$$

in which Φ_{TOC} is the quantum yield of TOC and $k_{O_3,TOC}$ is the rate constant for reaction of TOC with ozone. Φ_{TOC} for natural organic matter as TOC using UV can vary significantly and is dependent on experimental conditions including quantum yield (related to organic matrix) and properties of the UV reactor system (12,13,21,36). The quantum yield of various organic compounds at 254 nm has been assessed in a literature review, with a range of $1.3*10^{-5}$ to 1.25 mol/Einstein (37). On the other hand, ozone is able to rapidly oxidize some organic matter, particularly olefins and aromatic rings. Ozone reaction rates with olefins and aromatic rings can reach up to 10^6 - 10^9 $M^{-1}s^{-1}$ for transformation of these compounds, while reaction rates between the other organic compound and ozone ranges between 10^{-5} – 10^1 $M^{-1}s^{-1}$ (12,38). Thus, ozone exhibits an overall low total organic carbon removal in most scenarios (38). Also, formation of hydroxyl radical through the direct ozone pathway and ozone scavenging by TOC (12,39,40) were considered negligible due to the expected low ozone concentration after immediate reaction with UV and hydrogen peroxide.

Modeling was conducted to solve for the rate constant $k_{OH^o,TOC}$, varying the values of the other model parameters, and comparing the fitted values to values obtained from the literature. Modeling was performed using Matlab Simulink 2017a, by optimization of the selected variables to achieve the lowest overall S-value (standard error of regression). The Combvec command was used to produce all possible variable combinations from variables either linearly or logarithmically spaced in their selected range with the linspace or logspace commands. The overall S-value minimized was the sum of the S-values from the hydrogen peroxide model fit and the TOC model fit.

3. Results

While pseudo-first order models were able to be fitted to data on ozone-UV TOC mineralization over a limited range, the value of the first-order rate constant obtained was found to be quite sensitive to the initial concentration. This lack of applicability is due to competition between organics and ozone for reaction with UV radiation in the first step of •OH generation, and to the competition between UV radiation and hydrogen peroxide for reaction with ozone in the second step (the latter not existing in the peroxone and UV-hydrogen peroxide processes). To model the mineralization of TOC by the ozone-UV process, a set of somewhat simplified rate equations governing the oxidation of TOC in the ozone-UV process were developed based on Equations 1 – 20, as follows:

$$\frac{d[O_3]}{dt} = [O_3]_{dose} - \Phi_{O_3} P_{UV} f_{O_3}\{1 - \exp(-2.3A)\} - k_{chain}[O_3] - k_{O_3,OH\bullet}[^{\bullet}OH][O_3] - 10^{pH-pK}[O_3][H_2O_2] \quad (21)$$

$$\frac{d[H_2O_2]}{dt} = \Phi_{O_3} P_{UV} f_{O_3}\{1 - \exp(-2.3A)\} - \Phi_{H_2O_2} I_0 f_{H_2O_2}\{1 - \exp(-2.3A)\} - k_{H_2O_2} 10^{pH-pK}[O_3][H_2O_2] - k_{H_2O_2,OH\bullet}[^{\bullet}OH][H_2O_2] \quad (22)$$

$$\frac{d[^{\bullet}OH]}{dt} = 2\Phi_{H_2O_2} P_{UV} f_{H_2O_2}\{1 - \exp(-2.3A)\} + k_n 10^{pH-pK}[O_3][H_2O_2]^{0.5} - k_{H_2O_2,O}[^{\bullet}OH] - k_{O_3,OH\bullet}[O_3][^{\bullet}OH] - k_{OH\bullet,TOC}[^{\bullet}OH][TOC] - k_{11}[HCO_3^-][OH\bullet] \quad (23)$$

$$\frac{d[TOC]}{dt} = -k_{OH\bullet,TOC}[^{\bullet}OH][TOC] - \Phi_{TOC} P_{UV} f_{TOC}(1 - \exp(-2.3A)) - k_{O_3,TOC}[O_3][TOC] \quad (24)$$

in which $[O_3]_{dose}$ is the ozone concentration delivered to the water in the reactor per unit time (93% of the gaseous ozone under the experimental conditions, according to manufacturer

graphical data), k_{chain} is the rate constant for ozone decay promoted by the $^{\bullet}O_2^-$ cyclic chain reaction (13), assuming that $^{\bullet}O_2^-$ concentration is nearly constant, and $k_{OH\bullet,TOC}$ is the rate constant of TOC with hydroxyl radical. High pH reactions were excluded in this model, as pH was between 5.5-7.5 during experiments.

Results of the calculated ε_{TOC} and measured pH input into the model are shown in Figure 2. The extinction coefficient for TOC appeared to increase with treatment time in each experiment, which seems to be consistent with the literature, where recalcitrant compounds also tend to absorb more UV light at 254 nm (37). TOC mineralization and H_2O_2 results during Runs 1 and 2 are shown in Figure 3, with Runs 3 and 4 in Figure 4. In all plotted results, H_2O_2 is modeled using the shifting pH data from the experiments, as opposed to the common assumption of a constant pH in AOP models. However, because the pH sensor malfunctioned during one experiment, the pH in figure 3(a) was calculated by the model so as to produce best-fit H_2O_2 and TOC projections. As shown, the result followed the same pH trend as the runs of Figure 3(b). Noting that actual shower runs were recorded starting at the end of a two-hour shower and treatment period, such that the final pH was recorded after six hours, whereas the final pH in the simulated runs was recorded after two hours, the overall decreasing/increasing trend observed is similar for simulated and actual shower runs. This trend is explained by CO_2 production and dissolution early, when TOC is mineralized most rapidly, followed by continual CO_2 stripping by O_2 injected at the venturi. However, initial pH was somewhat lower in actual shower runs (~7.3 versus ~6.9), perhaps due to the acidity of human skin surface pH, indicating that soybean oil alone may not be the best simulation of body organics washed off during showers (41).

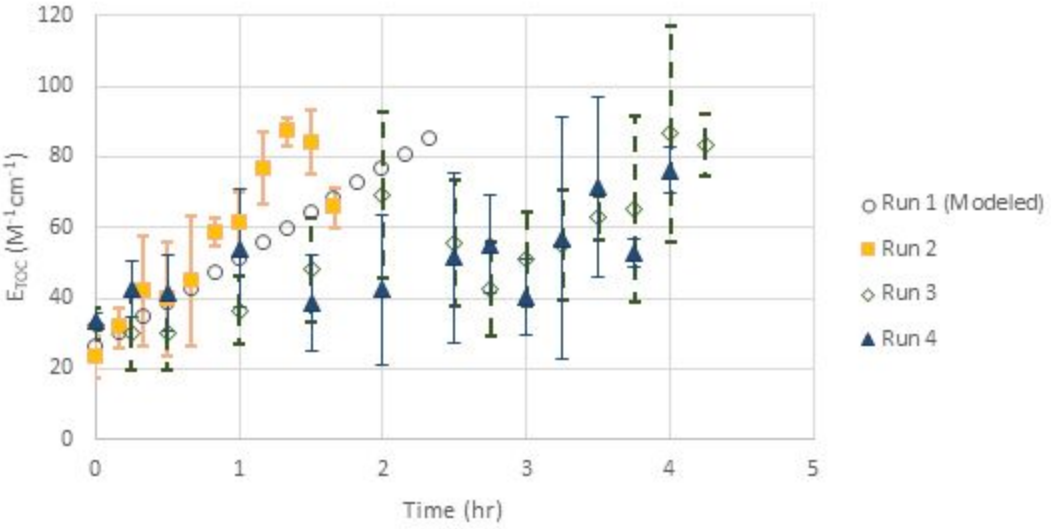

(a)

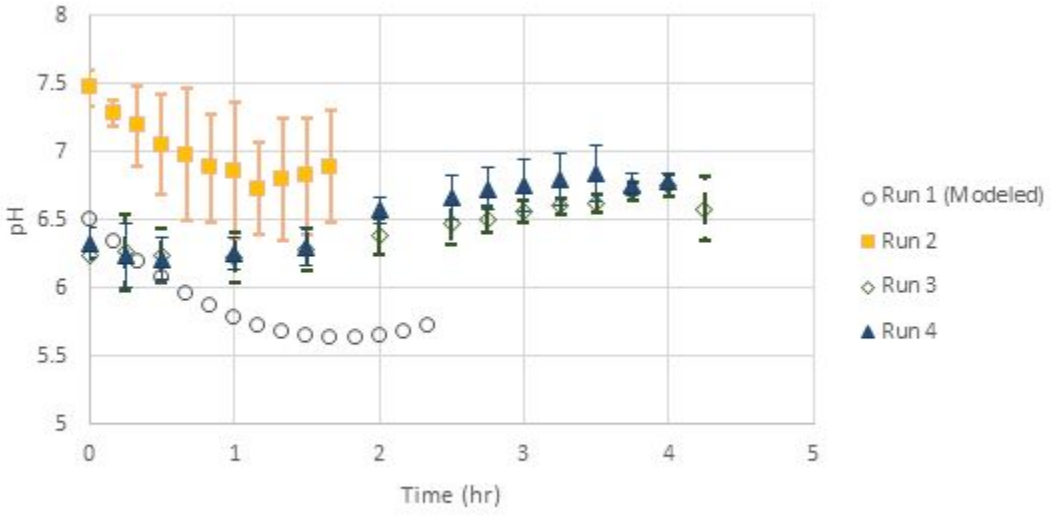

(b)

Figure 2. Calculated ε_{TOC} (a) and measured pH (b) for all experimental Runs.

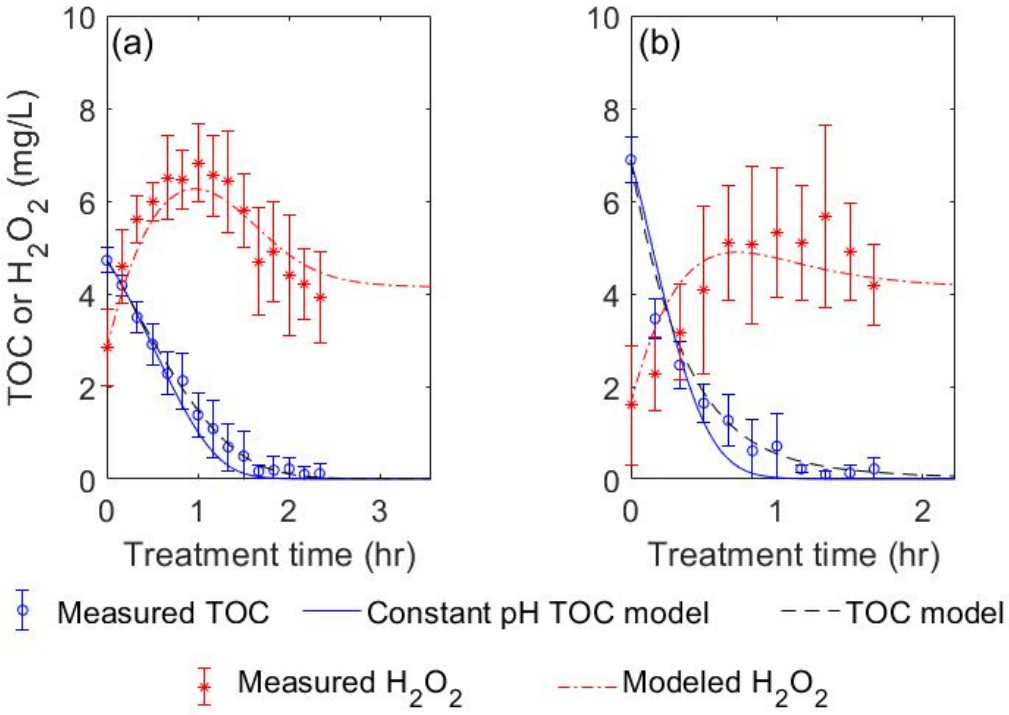

275

276 Figure 3. TOC and hydrogen peroxide model results and data points for batch runs of simulated
277 shower mixtures (showerhead was not used) (a) Run 1, and (b) Run 2. [Conditions: (a) Electrical
278 conductivity = 115 μS/cm, alkalinity = 10 mg/L, initial turbidity = 0.53 NTU, final turbidity =
279 0.12 NTU; (b) Electrical conductivity = 197 μS/cm, alkalinity = 25 mg/L, initial turbidity = 2.1
280 NTU, final turbidity = 0.14 NTU]

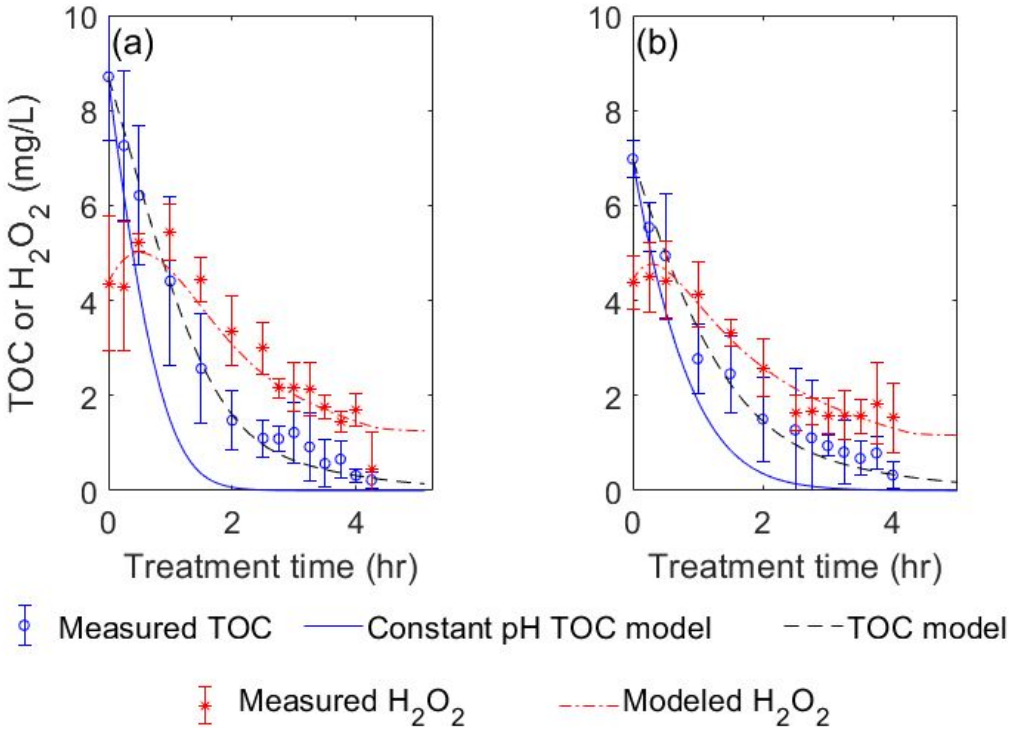

Figure 4. TOC and hydrogen peroxide model results and data points for actual shower runs with soap and conditioner (a) Run 3, (final data point indicates passing through GAC, not included in the S-value fit, and (b) Run 4. [Conditions: (a) Electrical conductivity = 197 μS/cm, alkalinity = 30 mg/L, initial turbidity = 0.61 NTU, final turbidity = 0.18 NTU; (b) Electrical conductivity = 214 μS/cm, alkalinity = 29 mg/L, initial turbidity = 1.64 NTU, final turbidity = 0.13 NTU]

In this study, pH evolved significantly during treatment due to ongoing mineralization of organics to CO_2. In particular, it was theorized that produced CO_2 gas would dissolve in, and acidify, the water, and then be stripped towards equilibrium with the incoming gas mixture comprising oxygen, nitrogen, and ozone resulting from the ozone injection process. This process of equilibration would be relatively slow due to the coarse and localized nature of the bubbles entering the tank and would evolve in response to changes in the production of CO_2 from TOC in the water. Because water was circulating in the tank, a minor additional effect was theorized due to the shifting concentration of CO_2 gas above the water in the tank, which in turn would evolve in response to gases leaving through the ozone vent and gas entering due to both ozone

296 generation and TOC mineralization. Some time after treatment was concluded, the equilibrium
297 was expected to be reached with the CO_2 in the ozone production gas still being injected, likely
298 lower than atmospheric CO_2 concentration due to the oxygen concentrator component of the
299 ozonation system and based on correspondence with the manufacturer.

300 The evolution of process pH was not successfully modeled using carbonate equilibrium
301 and kinetic relationships, due to uncertainties in reactor-specific liquid and gas-phase hydraulics
302 and liquid-gas mass transfer. Therefore, pH was monitored experimentally and entered as input
303 to the model, whereas pH has previously been constant, held constant, or assumed constant
304 during experiments (13,21,42–44). In addition, many models do not assess the impact of changing
305 organic concentration on UV absorbance, which can be substantial at high organic loading
306 (13,17,18).

307 Results of modeling shown in Figures 3 and 4 indicate that the oxidation efficiency of the
308 ozone-UV system is governed principally by TOC loading and pH, with TOC loading controlling
309 UV transmissivity of the water, and high pH increasing hydrogen peroxide ionization necessary
310 for the generation of hydroxyl radical in the peroxone reactions. The latter effect was apparently
311 so strong that experimental results could not be adequately predicted without accounting for the
312 evolution in pH over the course of treatment. That is, assuming pH to remain constant at the
313 value measured before showers occurred resulted in significant over-prediction of TOC
314 mineralization in all cases.

315 At most rates of ozone oxidation and UV photolysis tested, model results indicated that
316 these mechanisms were not significant compared with hydroxyl radical degradation of organics.
317 In particular, the best fits obtained had nearly the same S-value in all cases, with no change in
318 fitted parameter values other than the rate constants for oxidation by ozone and UV photolysis.

This result indicates that those mechanisms had little impact on TOC mineralization, likely because dissolved ozone concentration was too low, and while organic compounds absorbed a high percentage of UV light, UV photolysis was not important. This result is in agreement with previous studies, in which UV provided little to no degradation of natural organic matter, ozone alone was generally slower than hydroxyl radical degradation, and little dissolved ozone residual was present during ozone-UV advanced oxidation (12,13,36,45–47).

Direct oxidation by UV began to have a modeled effect at a quantum yield of 0.1 mol/Einstein. This is on the high end of the range reported previously for specific organic components. In addition, equation 19 assumes that the total quantity of the organics may be oxidized directly by UV, which is unlikely. Therefore, it is assumed that direct UV degradation of the organic matter is negligible, though future studies should assess this in more detail. Direct oxidation by ozonation began to have a modeled effect at a second order rate constant of $1*10^3$ $M^{-1}s^{-1}$. This rate constant seems to be significantly higher than literature rate constants for ozone mineralization of TOC, but is lower than the transformation rate constants. Equation 20 also assumes that the full quantity of organics may be mineralized by ozone. Based on this assessment, it is unlikely that direct ozone mineralization has a significant effect on TOC mineralization under these conditions, though further study should confirm that. The only other tested variable not affecting model fit was $k_{H_2O_2,O_3}$, evaluated by the same method as UV photolysis and ozone oxidation. Therefore, $k_{H_2O_2,O_3}$was set to equal $2.2*10^6$ $M^{-1}s^{-1}$ (Table 2), and UV photolysis and ozone oxidation were assumed negligible, to obtain final results listed in Table 2.

339 Table 2. Model Results and Comparison with Literature Values for Variables

Variable	Literature value	Simulated run no conditioner model value	Simulated run with conditioner model value	Shower run with GAC model value	Shower run without GAC model value	Reference for literature value
b	-	16 cm	10 cm	9.65 cm	9.65cm	-
k_{chain}	0.5 s^{-1}	1.5 s^{-1}	2.8 s^{-1}	2.8 s^{-1}	1.5 s^{-1}	(13)
$k_{O_3,OH\bullet}$	$3.0*10^9$ $M^{-1}s^{-1}$	$2.5*10^9$ $M^{-1}s^{-1}$	$3.0*10^9$ $M^{-1}s^{-1}$	$3.0*10^9$ $M^{-1}s^{-1}$	$3.0*10^9$ $M^{-1}s^{-1}$	(22)
$k_{H_2O_2,O_3}$	$2.2*10^6$ $M^{-1}s^{-1}$	$2.2*10^6$ $M^{-1}s^{-1}$	$2.2*10^6$ $M^{-1}s^{-1}$	$2.2*10^6$ $M^{-1}s^{-1}$	$2.2*10^6$ $M^{-1}s^{-1}$	(18)
$k_{H_2O_2,OH\bullet}$	$2.7*10^7$ $M^{-1}s^{-1}$	$2.0*10^7$ $M^{-1}s^{-1}$	$3.5*10^7$ $M^{-1}s^{-1}$	$2.0*10^7$ $M^{-1}s^{-1}$	$3.5*10^7$ $M^{-1}s^{-1}$	(35)
k_n	$4.0*10^6$ $M^{-0.5}s^{-1}$	$4.0*10^7$ $M^{-0.5}s^{-1}$	$4.0*10^7$ $M^{-0.5}s^{-1}$	$7.6*10^7$ $M^{-0.5}s^{-1}$	$7.6*10^7$ $M^{-0.5}s^{-1}$	(13)
$k_{OH\bullet,TOC}$[a]	$1*10^4$ - $1*10^{11}$ $M^{-1}s^{-1}$	$7.6*10^7$ $M^{-1}s^{-1}$	$6.4*10^7$ $M^{-1}s^{-1}$	$2.2*10^7$ $M^{-1}s^{-1}$	$1.7*10^7$ $M^{-1}s^{-1}$	(4,6,12)
S-value	-	0.553 mg/L	0.997 mg/L	0.638 mg/L	0.549 mg/L	-

340 [a]Range includes single organic compounds in pure water, organic mixtures in surface waters or pure waters, and mixed organics in
341 secondary effluent

342 For the all runs, model-predicted concentrations of dissolved ozone and hydroxyl radical
343 (not measured experimentally) are shown in Figures 5-6, while the modeled fractions of UV light
344 absorbed by the three UV absorbing constituents, ozone, hydrogen peroxide, and TOC, are shown
345 in Figure 7-8. The hydroxyl radical concentration predicted by the model is similar to hydroxyl
346 radical concentrations expected in water treatment using advanced oxidation processes (12,13).

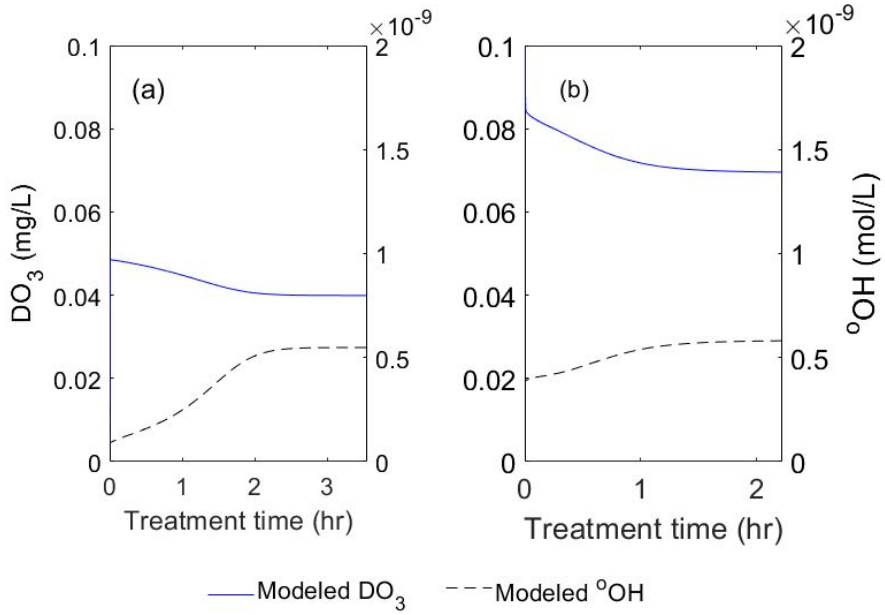

347

348 Figure 5. Modeled dissolved ozone and hydroxyl radical concentrations for Runs 1 (a) and 2 (b).

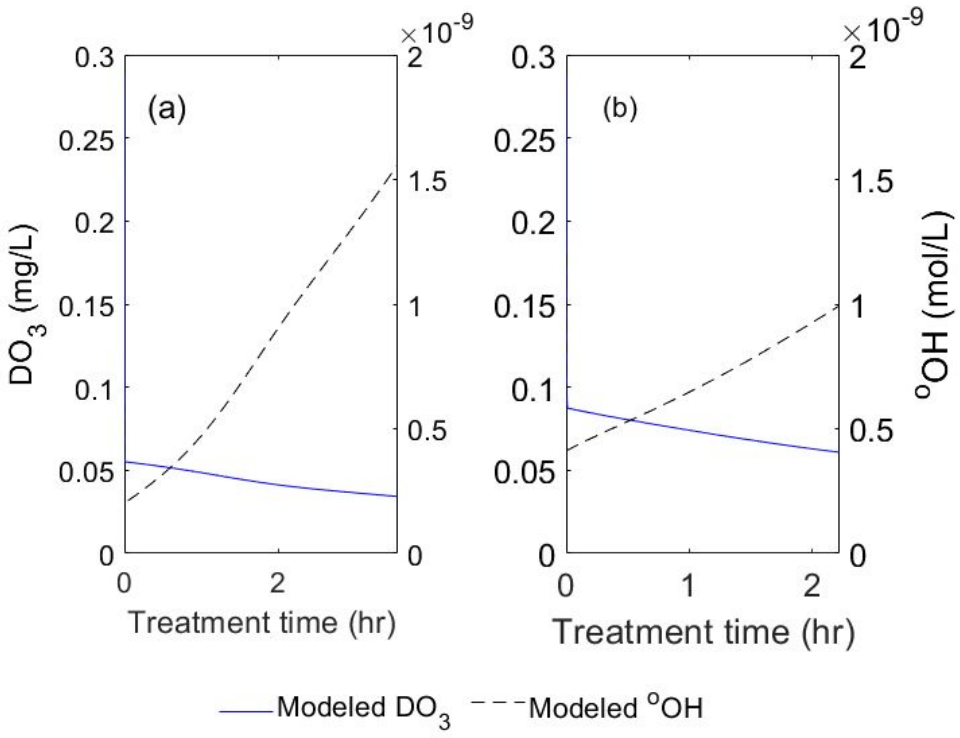

349

350 Figure 6. Modeled dissolved ozone and hydroxyl radical concentrations for Runs 3 (a) and 4 (b).

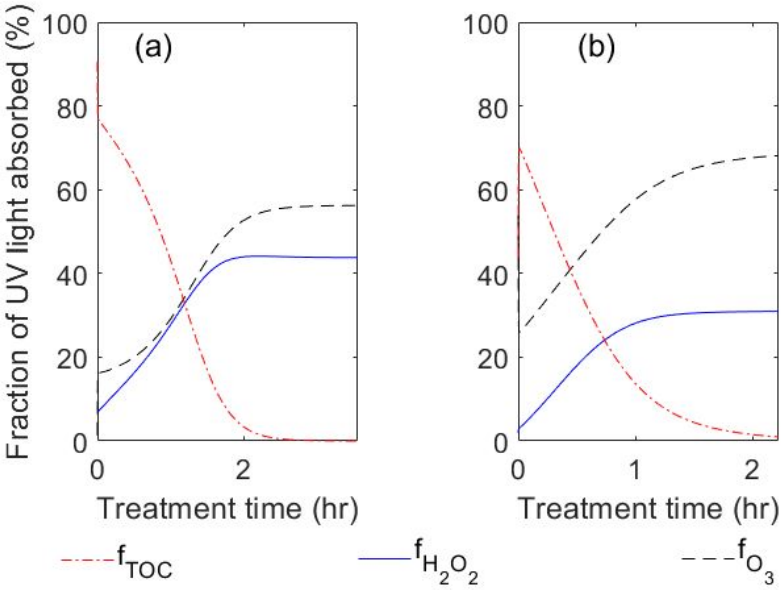

351

352 Figure 7. Modeled fractions of UV light absorbed by ozone, hydrogen peroxide, and TOC,
353 during Runs 1 (a) and 2 (b).

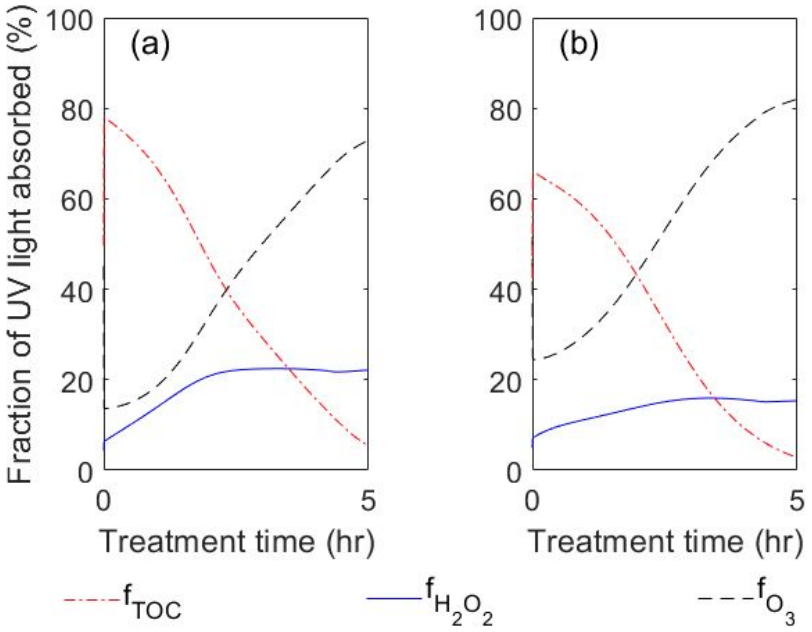

Figure 8. Modeled fractions of UV light absorbed by ozone, hydrogen peroxide, and TOC, during Runs 3 (a) and 4 (b).

Differences in the trends shown in H_2O_2 and •OH in Figures 5 – 8 can be explained by the trends in pH shown in Figures 3 and 4. That is, in Runs 1 and 2, both pH and TOC were decreasing with treatment time, resulting in a relatively steady aqueous hydrogen peroxide concentration and hydroxyl radical concentration throughout the treatment period, and a lowered oxidation capacity compared to the Figure 4 runs. In contrast, during Runs 3 and 4, pH was increasing as TOC was decreasing, leading to a rapidly increasing hydroxyl radical concentration and decreasing aqueous hydrogen peroxide concentration through the treatment period, resulting in increased oxidation towards the end of the treatment period relative to Runs 1 and 2.

To illustrate the importance of the differences between the three run types due to pH and light path effects, the modeled ratio of hydroxyl radical production in the peroxone reactions to

368 the hydroxyl radical production in the UV-H_2O_2 reactions is presented in Figure 9. In Runs 1 and
369 2, this ratio is initially decreasing, because pH is decreasing during treatment, reducing the
370 availability of ionized H_2O_2, thus increasing the importance of the UV-H_2O_2 reactions, which
371 utilize aqueous H_2O_2.. In Runs 3 and 4, pH was increasing during the entire treatment period after
372 showers, increasing the hydroxyl radical production due to peroxone reactions, because more
373 ionized H_2O_2 was available.

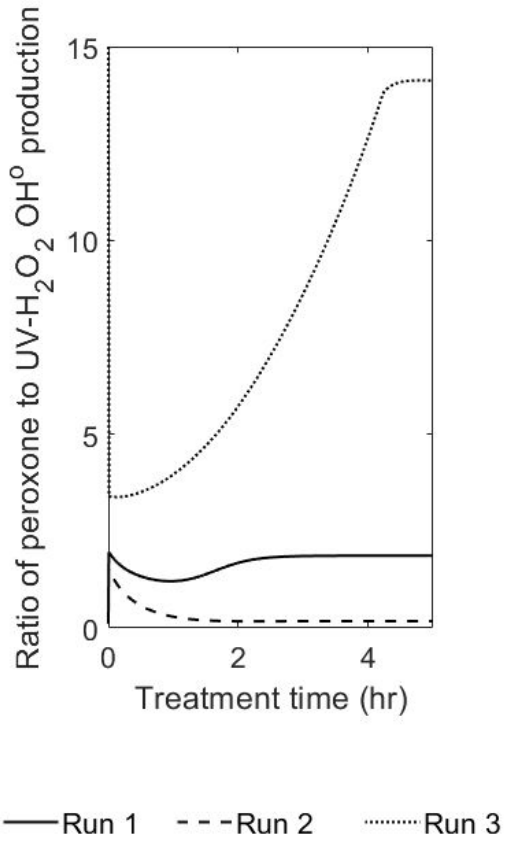

374
375 Figure 9. Predicted ratio of peroxone to UV-H_2O_2 hydroxyl radical production. Result for Run 4
376 was essentially identical to Run 3 and is not plotted.
377
378 The model developed and calibrated with pilot data was used to evaluate the EEO, or
379 electrical energy per order of magnitude organics mineralization (kWh/m^3/order), of the ozone-
380 UV process for mineralization of TOC, as a function of ozone and UV dose, for the experimental
381 conditions of this work and the published electrical requirements of commercial ozone-UV

382 equipment. Results are presented in Figure 10 for dose combinations within one order of
383 magnitude of the experimental dose, assuming UV power was equal to UV lamp power + 100 W
384 for the controller, and ozone power at 12 kWh/kg ozone generated (48,49), with 93% transfer
385 efficiency. Of note, the ozone energy assumption used is for larger scale ozone equipment (>~750
386 g/hr generation; (49)). For a single shower system at 32 showers/day, the ozone generation energy
387 would be 2.5 times higher due to constant oxygen concentrator energy. In Figure 10, the bottom
388 shading indicates values that were below 5 kWh/m^3/order.

389 Based on the results shown in Figure 10, increasing or decreasing either ozone or UV dose
390 while holding the other constant past a certain point will result in greatly increased EEO. The
391 dose used in this study, 25 g/hr ozone and 600 W UV, was within 20% of the predicted minimum
392 EEO (4.42 kWh/m^3/order predicted experimental EEO, versus 3.73 kWh/m^3/order predicted
393 minimum EEO), at the experimental ozone:UV dose ratio of 0.18 ($8.82*10^{-6}$ mol/L/s:$5.06*10^{-5}$
394 einstein/L/s). Results suggest that, given the UV lamp power available for this work, ozone dose
395 could have been increased further to provide reduced treatment time at only a minor increase in
396 EEO. For comparison, other studies have documented dose ratios in the range of 0.1-2 ozone:UV
397 (mol/L/s:einstein/L/s), for removal of NOM or specific organic compounds in varying water
398 matrices (12,13,18–22,42).

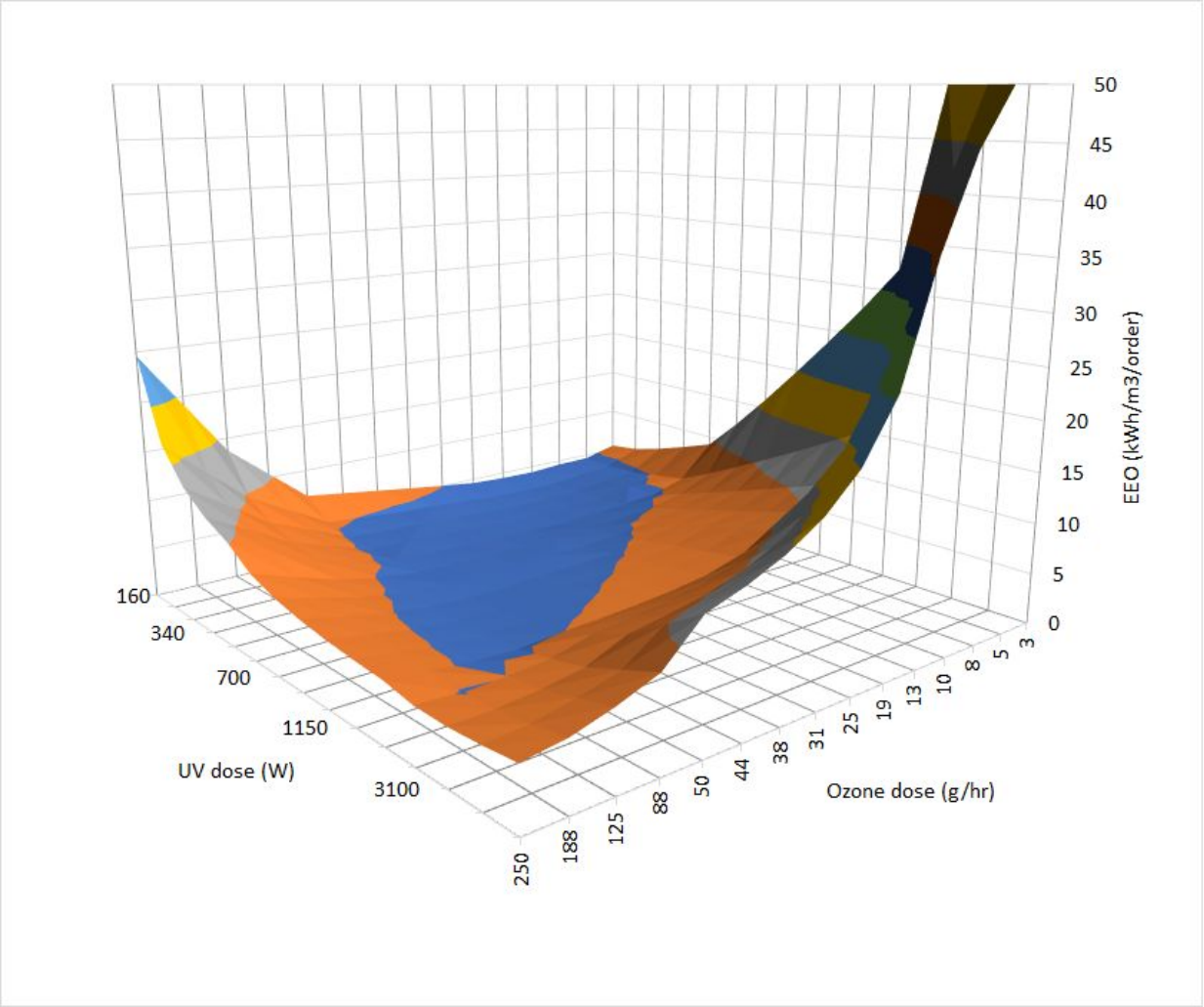

Figure 10. Modeled effect of changing ozone and UV dose on treatment efficiency (EEO). The bottom shaded region indicates EEO values less than 5 kWh/m^3/order.

4. Discussion

While results agreed well with pilot data and literature reports, the model-predicted value of k_n, the net rate constant for peroxone production of hydroxyl radical, was significantly higher than that obtained in Soo Oh et al. (2005). This result may be due to the difference in water matrix, as k_n was determined by the authors in pure water. Perhaps more important, the difference could be due to reactor design and dosing. That is, Soo Oh et al. (2005) experiments were at bench scale, using an inline ozone mixer and UV lamp in a continuously stirred reactor, while the experiments detailed in this study were conducted in a recirculating reactor with venturi ozone injection and

411 UV reactors with highly reflective reaction chambers designed to ensure that all UV light is
412 absorbed. These factors may have increased hydroxyl radical generation and reaction efficiency.
413 Also, the authors appeared not to account for total solution absorbance in the terms 1-exp(-2.3A)
414 (Equations 18 – 20), and calibrated and demonstrated the model only for H_2O_2 and ozone without
415 quantitative consideration of natural organic matter in the water.

416 Lack of direct oxidation by photolysis and ozone may have been expected, because direct
417 ozone decomposition of natural organic matter is typically 3-5 times slower than degradation of
418 NOM in the ozone-UV process, and not all organics will be degraded without an unreasonably
419 long treatment time (12,13,21). In addition, dissolved ozone concentration during the ozone-UV
420 process is typically low due to the cyclic decay reactions and reactions with UV, H_2O_2, and
421 hydroxyl radical. Finally, UV at 254 nm provides little to no degradation of natural organic matter
422 on its own, and less lamp power is available for photolysis of organics in ozone-UV compared to
423 UV alone due to additional absorption by ozone and H_2O_2 (13,36).

424 Significant difference in model parameters between different scenarios occurred only for
425 the mineralization rate constant of hydroxyl radical reacting with TOC. Second order rate
426 constants fitted to the data obtained with model Equation 24 ranged from $1.7–7.6*10^7$ $M^{-1}s^{-1}$. The
427 result from the simulated runs is similar to those reported for mineralization of wastewater using
428 hydroxyl radical generating processes, and approximately three times lower than that reported for
429 natural organic matter (4,12,50,51). The results from the actual shower runs are similar to reported
430 rate constants for the advanced oxidation of biologically-treated municipal wastewater, and an
431 order of magnitude lower than reported for natural organic matter (4,12,50). The relatively low
432 value obtained in the latter case may be attributed to the composition of the conditioner or soap
433 or both, though no published rate constants for reaction of hydroxyl radical with the principal

specific organic components of conditioner were found, and Campsuds ingredients are not publicly available.

A t-test indicated that the values of $k_{OH\bullet,TOC}$ in the simulated shower runs ([7.6 ± 0.77]*10^7 $M^{-1}s^{-1}$ without conditioner, 6.4 ± 0.47]*10^7 $M^{-1}s^{-1}$ with conditioner) compared to the actual shower runs ([2.0 ± 0.35]*10^7 $M^{-1}s^{-1}$) were significantly different ($p < 0.001$). This result suggests that the 2-hour period of treatment while showers were occurring significantly affected the overall rate of organic reaction with hydroxyl radical. Some organics present in the greywater mixture likely oxidized quickly during the initial two-hour period while showers were occurring, and the more recalcitrant organics were treated in the remaining four-hour treatment period that followed the two hours of showers.

Initial pH and pH changes during treatment are predicted to have a strong impact on the mineralization efficiency of the ozone-UV process. The ozone-UV process has proven effective for pH varying from ~4 – 9, though optimal dosing ratios of ozone:UV may vary with pH. For example, in Soo Oh et al. (2005), at pH 4, the range of optimal dosing ratios for the goal of UV_{254} reduction is much narrower than at pH 7, though it is still possible to achieve approximately the same rate of UV_{254} reduction at both pH values, provided dosing ratio is optimized (13). Because the dominant hydroxyl radical production mechanism at pH 4 would be UV-H_2O_2, it is reasonable that a higher ozone dose at pH 4 would decrease efficiency, as ozone would block UV light from interacting with H_2O_2, while hydroxyl radicals that do form would be split in reactions with organics and high H_2O_2/O_3 concentrations. Therefore, higher ozone:UV dosing ratios would not be efficient at low pH, compared to the same ratio at neutral pH. Another study reports an increase in oxidation of fluorene from pH 2-7 and decrease from 7-12 (43). While not important to the present process or included in this model, high pH reactions should be considered starting around

457 pH 9. These include competitive reaction of O_3 with OH^- either to a decay reaction or to form
458 hydroxyl radical, both resulting in reduced O_3 availability for peroxone reactions, and the
459 dissociation of hydroxyl radical to oxygen anion radical (21,43,44,52). These reactions, when
460 combined, appear to cause an overall decrease in hydroxyl radical production at high pH values
461 (21,43,44,52).

462 The range of predicted EEO values falling within 20% of the minimum occurred at
463 ozone:UV ratios varying from 0.14-1.05 (mol/L/s:einstein/L/s), using dose combinations of
464 ozone and UV ranging from 20% to 750% of the experimental dose. Hence, at least for the system
465 described, treatment can be accelerated or slowed by increasing or decreasing dose, without
466 affecting energy efficiency, by maintaining the appropriate dose ratio within this range. Thus,
467 capital cost can be minimized subject to footprint, operating requirements, and other constraints.

468 The predicted EEO for the ozone-UV process can be compared with the peroxone
469 process, at 2 kWh/m^3/order (3), UV-H_2O_2 at 7.0 kWh/m^3/order (4), and UV-TiO_2 at 6.5
470 kWh/m^3/order (53). Thus, at an EEO of ~4.42 kWh/m^3/order, ozone-UV consumes less energy
471 than other UV-based AOPs, but more than the peroxone process, because generation of hydrogen
472 peroxide through the anthraquinone process is more energy efficient than UV generation of
473 hydrogen peroxide (12), whereas inclusion of the peroxone reactions increases efficiency relative
474 to other UV-based processes.

475 The ability to alter the dose ratio within a range while maintaining a constant energy
476 consumption has interesting implications for treatment. First, aqueous H_2O_2 formation and
477 discharge may be controlled by adjusting the dose ratio, potentially alleviating the need to quench
478 H_2O_2 prior to downstream disinfection, to prevent consumption of chlorine (10). Additionally, a
479 reduction in ozone and increased UV dose may aid in mitigation of bromate, a carcinogenic

product of ozonation. Dose ratio might also be adjusted to optimize the intrinsic overall, or organism-specific, disinfection capacity of the ozone-UV process itself.

5. Conclusions

The ozone-UV kinetic model presented was demonstrated to predict hydrogen peroxide and TOC concentrations in greywater reuse treatment, while providing information on expected ozone and hydroxyl radical concentrations in the water. The model accounts for competition between organics and ozone for reaction with UV radiation in the first step of •OH generation, and competition between UV radiation and hydrogen peroxide for reaction with ozone in the second step. Besides their importance in predicting treatment efficiency, an understanding of these interactions is also important because they limit the UV and ozone available for disinfection, and affect the extent of reaction of ozone to produce unwanted byproducts such as bromate, and impact residual H_2O_2 in the effluent which may quench added chlorine disinfectant. Additionally, if •OH scavengers are present (H_2O_2, O_3, and alkalinity in the conditions tested), then ozone-UV dosing ratio can have a significant impact on bromate formation potential (54). The model was also useful in predicting energy efficiency as a function of UV and ozone dose, based on published energy requirement for commercial ozone and UV reactors.

Conclusions based on this study include:

- Direct photolysis, direct ozone oxidation, and ozone formation of hydroxyl radical were not considered as important contributors to TOC mineralization in greywater by the ozone-UV process in this model;
- The second-order rate constant for hydroxyl radical mineralization of greywater TOC was assessed as $[7.6 \pm 0.77]*10^7$ $M^{-1}s^{-1}$ without conditioner, $6.4 \pm 0.47]*10^7$ $M^{-1}s^{-1}$ with conditioner during simulated shower batch runs and $[2.0 \pm 0.35]*10^7$ $M^{-1}s^{-1}$ during actual

503 shower fed batch runs, with the two-hour treatment period while showers were occurring
504 in the actual shower runs having a significant impact on the rate constant for the four-
505 hour treatment period after showers ended;

506 • The efficiency of TOC mineralization by the ozone-UV process is governed by TOC
507 concentration (controlling transmissivity) and pH throughout treatment, and ozone-UV
508 dose ratio. In particular, process pH evolves during treatment as a function of TOC
509 mineralization/reactor hydraulics, while the molar absorptivity of TOC tended to increase
510 with treatment time, indicating compounds recalcitrant to advanced oxidation absorbed
511 more UV light;

512 • While existing models have assumed constant pH, mineralization of greywater TOC
513 produces sufficient CO_2 to depress pH and treatment efficiency. Hence, if constant pH
514 is assumed, a lower projected average pH value should be used. In the current work,
515 experimental data on pH over the course of treatment was required as input, accounting
516 for the relatively strong effect of pH while maintaining the generality of the model to
517 different reactor designs and conditions; and

518 • The minimum EEO assessed at dose combinations within one order of magnitude of the
519 experimental dose, for greywater TOC mineralization by the ozone-UV system described
520 in this paper is 3.73 kWh/m^3/order, and the ozone:UV dose ratio and the magnitude of
521 the doses could be altered within a range (120- 3000 W UV and 7.5-188 g/hr ozone, with
522 ozone:UV ratios ranging from 0.14-1.05 in this study) without significantly changing EEO.

523 • The addition of carbonate equilibrium calculations to account for changes in pH
524 dynamically in the model would be useful as a basis for the design of TOC
525 mineralization processes, if alkalinity contained in the influent greywater is accounted for;

- Additional detailed assessment of reactions including direct TOC mineralization by UV and ozone, ozone hydroxyl radical formation, and scavenging of TOC by ozone is recommended to improve model capabilities;

Conflicts of Interest

There are no conflicts to declare.

Acknowledgements

This work was supported by the National Science Foundation under Grant Nos. 1519058 and 1038257. In addition, contributions by the University of Miami and Engineered Control Systems, Inc. are gratefully acknowledged. The authors would also like to thank Spartan Environmental Technologies for technical collaboration, and the 16 student research assistants who helped with system fabrication, operation, sampling, analysis, and data processing.

References

1. Rodriguez C, Van Buynder P, Lugg R, Blair P, Devine B, Cook A, et al. Indirect potable reuse: A sustainable water supply alternative. Int J Environ Res Public Health [Internet]. 2009 Mar 17;6(3):1174–203. Available from: http://www.mdpi.com/1660-4601/6/3/1174/
2. WateReuse Research Foundation, American Water Works Association, Water Environment Federation, National Water Research Institute, Tchobanoglous G, Cotruvo J, et al. Framework for Direct Potable Reuse [Internet]. Mosher JJ, Melin Varaniani G, editors. Alexandria: WateReuse Research Foundation; 2015. Available from: http://www.nwri-usa.org/pdfs/DPR-Framework----FINAL.pdf
3. Wu T, Englehardt JD. Peroxone mineralization of chemical oxygen demand for direct potable water reuse: Kinetics and process control. Water Res. 2015;73:362–72.
4. Gassie LW, Englehardt JD, Wang J, Brinkman N, Garland J, Gardinali P, et al. Mineralizing urban net-zero water treatment: Phase II field results and design recommendations. Water Res [Internet]. 2016 Nov;105:496–506. Available from: http://linkinghub.elsevier.com/retrieve/pii/S0043135416306820
5. Squire D. Reverse osmosis concentrate disposal in the {UK}. Desalination [Internet]. 2000;132(1–3):47–54. Available from: http://www.sciencedirect.com/science/article/pii/S001191640000134X
6. Wu T, Englehardt JD. Mineralizing urban net-zero water treatment: Field experience for energy-positive water management. Water Res. 2016;106:352–63.
7. Pérez-González A, Urtiaga AM, Ibáñez R, Ortiz I. State of the art and review on the treatment technologies of water reverse osmosis concentrates. Water Res [Internet]. 2012;46(2):267–83. Available from: http://linkinghub.elsevier.com/retrieve/pii/S0043135411006440

8. Zhao Y, Song L, Ong SL. Fouling behavior and foulant characteristics of reverse osmosis membranes for treated secondary effluent reclamation. J Memb Sci [Internet]. 2010;349(1–2):65–74. Available from: http://linkinghub.elsevier.com/retrieve/pii/S0376738809008345

9. Pearce GK. UF/MF pre-treatment to RO in seawater and wastewater reuse applications: a comparison of energy costs. Desalination [Internet]. 2008 Mar;222(1–3):66–73. Available from: http://linkinghub.elsevier.com/retrieve/pii/S0011916407007564

10. Gassie LWLW, Englehardt JDJD. Advanced oxidation and disinfection processes for onsite net-zero greywater reuse: A review. Water Res [Internet]. 2017 Nov;125:384–99. Available from: http://linkinghub.elsevier.com/retrieve/pii/S0043135417307261

11. Guo T, Englehardt JD. Principles for scaling of distributed direct potable water reuse systems: A modeling study. Water Res [Internet]. 2015 May;75:146–63. Available from: http://linkinghub.elsevier.com/retrieve/pii/S0043135415001062

12. Crittenden JC, Trussell RR, Hand DW, Howe KJ, Tchobanoglous G. MWH's Water Treatment [Internet]. 3rd ed. Hoboken, NJ, USA: John Wiley & Sons, Inc.; 2012. Available from: http://doi.wiley.com/10.1002/9781118131473

13. Soo Oh B, Kim SK, Kang MG, Oh JH, Kang J-W. Kinetic study and optimum control of the ozone/UV process measuring hydrogen peroxide formed in-situ. Ozone Sci Eng. 2005;27:421–30.

14. Purifics. Purifics' Photo-Cat cleans up contaminated groundwater. Membr Technol [Internet]. 2011;2011(9):6. Available from: http://ac.els-cdn.com/S0958211811701768/1-s2.0-S0958211811701768-main.pdf?_tid=bc9ed3e8-18e3-11e5-8004-00000aab0f6c&acdnat=1434980390_1294f9ddea0b138ae009acf8e7843559

15. Sichel C, Garcia C, Andre K. Feasibility studies: UV/chlorine advanced oxidation treatment for the removal of emerging contaminants. Water Res [Internet]. 2011 Dec 1;45(19):6371–80.

585 Available from: http://www.ncbi.nlm.nih.gov/pubmed/22000058
586 16. Wang D, Bolton JR, Hofmann R. Medium pressure UV combined with chlorine advanced
587 oxidation for trichloroethylene destruction in a model water. Water Res [Internet]. 2012
588 Oct;46(15):4677–86. Available from:
589 https://linkinghub.elsevier.com/retrieve/pii/S0043135412004034
590 17. Peyton GR, Huang FY, Burleson JL, Glaze WH. Destruction of pollutants in water with
591 ozone in combination with ultraviolet radiation. 1. General principles and oxidation of
592 tetrachloroethylene. Environ Sci Technol [Internet]. 1982;16(8):448–53. Available from:
593 http://pubs.acs.org/doi/abs/10.1021/es00102a004
594 18. Peyton GR, Glaze WH. Destruction of pollutants in water with ozone in combination with
595 ultraviolet radiation. 3. Photolysis of aqueous ozone. Environ Sci Technol [Internet]. 1988
596 Jul;22(7):761–7. Available from: http://pubs.acs.org/doi/abs/10.1021/es00172a003
597 19. Glaze WH, Kang J-W, Chapin DH. The chemistry of water treatment processes involving
598 ozone, hydrogen peroxide and ultraviolet radiation. Ozone Sci Eng [Internet]. 1987
599 Sep;9(4):335–52. Available from:
600 http://www.tandfonline.com/doi/abs/10.1080/01919518708552148
601 20. Lamsal R, Walsh ME, Gagnon GA. Comparison of advanced oxidation processes for the
602 removal of natural organic matter. Water Res [Internet]. 2011 May;45(10):3263–9. Available
603 from: http://linkinghub.elsevier.com/retrieve/pii/S0043135411001564
604 21. Ratpukdi T, Siripattanakul S, Khan E. Mineralization and biodegradability enhancement of
605 natural organic matter by ozone–VUV in comparison with ozone, VUV, ozone–UV, and UV:
606 Effects of pH and ozone dose. Water Res [Internet]. 2010 Jun;44(11):3531–43. Available
607 from: http://linkinghub.elsevier.com/retrieve/pii/S0043135410002228
608 22. Langlais B, Reckhow D, Brink D. Ozone in Water Treatment. New York, NY: Lewis

609 Publishers; 1991.
610 23. Benami M, Gillor O, Gross A. Potential health and environmental risks associated with onsite
611 greywater reuse: A review. Built Environ. 2016;42(2):212–29.
612 24. Church J, Verbyla ME, Lee WH, Randall AA, Amundsen TJ, Zastrow DJ. Dishwashing water
613 recycling system and related water quality standards for military use. Sci Total Environ
614 [Internet]. 2015 Oct;529:275–84. Available from:
615 http://dx.doi.org/10.1016/j.scitotenv.2015.05.007
616 25. Ibrahim A, Alaziz A, Al-saqer NF. The Reuse of Greywater Recycling For High Rise
617 Buildings in Kuwait Country. Int J Eng Res Appl. 2014;4(3):208–15.
618 26. Leong JYC, Oh KS, Poh PE, Chong MN. Prospects of hybrid rainwater-greywater
619 decentralised system for water recycling and reuse: A review. J Clean Prod [Internet].
620 2016;142:3014–27. Available from: http://dx.doi.org/10.1016/j.jclepro.2016.10.167
621 27. Etchepare R, van der Hoek JP. Health risk assessment of organic micropollutants in
622 greywater for potable reuse. Water Res [Internet]. 2015;72:186–98. Available from:
623 http://dx.doi.org/10.1016/j.watres.2014.10.048
624 28. Gassie LW, Englehardt JD, Brinkman N, Garland J, Perera K. Ozone-UV net-zero water
625 wash station for remote emergency response healthcare units: Design, operation, and results.
626 Under Rev. 2019;
627 29. Gordon G, Cooper WJ, Rice RG, Pacey GE. Disinfectant Residual Measurement Methods.
628 2nd ed. Denver: AWWARF and AWWA; 1992.
629 30. American Public Health Association. Standard Methods for the Examination of Water and
630 Wastewater. 21st ed. Eaton, Andrew D., Franson MAH, editor. American Public Health
631 Association; 2005. 1200 p.
632 31. Watson K, Farré MJ, Knight N. Strategies for the removal of halides from drinking water

633 sources, and their applicability in disinfection by-product minimisation: A critical review. J
634 Environ Manage [Internet]. 2012;110:276–98. Available from:
635 http://dx.doi.org/10.1016/j.jenvman.2012.05.023
636 32. Iida T, Amano Y, Machida M, Imazeki F. Effect of surface property of activated carbon on
637 adsorption of nitrate ion. Chem Pharm Bull (Tokyo) [Internet]. 2013;61(11):1173–7. Available
638 from: http://www.ncbi.nlm.nih.gov/pubmed/24189304
639 33. Taube H. Photochemical reactions of ozone in solution. Trans Faraday Soc [Internet].
640 1957;53:656. Available from: http://xlink.rsc.org/?DOI=tf9575300656
641 34. Kang JW, Lee KH. A kinetic model of the hydrogen peroxide UV process for the treatment
642 of hazardous waste chemicals. Environ Eng Sci. 1997;14(3):183–92.
643 35. Glaze WH, Lay Y, Kang J-W. Advanced Oxidation Processes . A Kinetic Model for the
644 Oxidation Hydrogen Peroxide and U V Radiation. Ind Eng Chem Res. 1995;37:2314–23.
645 36. Imoberdorf G, Mohseni M. Degradation of natural organic matter in surface water using
646 vacuum-UV irradiation. J Hazard Mater [Internet]. 2011 Feb;186(1):240–6. Available from:
647 http://linkinghub.elsevier.com/retrieve/pii/S0304389410014123
648 37. Wols BAA, Hofman-Caris CHMHM. Review of photochemical reaction constants of organic
649 micropollutants required for UV advanced oxidation processes in water. Water Res [Internet].
650 2012 Jun;46(9):2815–27. Available from:
651 http://linkinghub.elsevier.com/retrieve/pii/S0043135412002102
652 38. Geluwe S Van, Braeken L, Bruggen B Van Der. Ozone oxidation for the alleviation of
653 membrane fouling by natural organic matter : A review. Water Res [Internet].
654 2011;45(12):3551–70. Available from: http://dx.doi.org/10.1016/j.watres.2011.04.016
655 39. Buffle MO, Schumacher J, Salhi E, Jekel M, von Gunten U. Measurement of the initial phase
656 of ozone decomposition in water and wastewater by means of a continuous quench-flow

system: Application to disinfection and pharmaceutical oxidation. Water Res. 2006;40(9):1884–94.

40. Buffle MO, Schumacher J, Meylan S, Jekel M, Von Gunten U. Ozonation and advanced oxidation of wastewater: Effect of O3 dose, pH, DOM and HO.-scavengers on ozone decomposition and HO . generation. Ozone Sci Eng. 2006;28(4):247–59.

41. Lambers H, Piessens S, Bloem A, Pronk H, Finkel P. Natural skin surface pH is on average below 5, which is beneficial for its resident flora. Int J Cosmet Sci [Internet]. 2006 Oct;28(5):359–70. Available from: http://doi.wiley.com/10.1111/j.1467-2494.2006.00344.x

42. Garoma T, Gurol MD, Osibodu O, Thotakura L. Treatment of groundwater contaminated with gasoline components by an ozone/UV process. Chemosphere [Internet]. 2008 Oct;73(5):825–31. Available from: http://linkinghub.elsevier.com/retrieve/pii/S000456350800859X

43. Beltran FJ, Ovejero G, Garcia-Araya JF, Rivas J. Oxidation of polynuclear aromatic hydrocarbons in water. 2. UV radiation and ozonation in the presence of UV radiation. Ind Eng Chem Res [Internet]. 1995 May;34(5):1607–15. Available from: http://pubs.acs.org/doi/abs/10.1021/ie00044a013

44. Fu P, Feng J, Yang H, Yang T. Degradation of sodium n-butyl xanthate by vacuum UV-ozone (VUV/O3) in comparison with ozone and VUV photolysis. Process Saf Environ Prot [Internet]. 2016 Jul;102:64–70. Available from: http://linkinghub.elsevier.com/retrieve/pii/S0957582016000379

45. Glaze WH, Peyton GR, Lin S, Huang RY, Burleson JL. Destruction of pollutants in water with ozone in combination with ultraviolet radiation. II. Natural trihalomethane precursors. Environ Sci Technol [Internet]. 1982 Aug;16(8):454–8. Available from: http://pubs.acs.org/doi/abs/10.1021/es00102a005

681 46. Olson TM, Barbier PF. Oxidation kinetics of natural organic matter by sonolysis and ozone.
682 Water Res [Internet]. 1994 Jun;28(6):1383–91. Available from:
683 http://linkinghub.elsevier.com/retrieve/pii/0043135494903050
684 47. Gottschalk C, Libra JA, Saupe A. Ozonation of Water and Waste Water [Internet].
685 Weinheim, Germany: Wiley-VCH Verlag GmbH & Co. KGaA; 2009. Available from:
686 http://doi.wiley.com/10.1002/9783527628926
687 48. U.S. Environmental Protection Agency. EPA Guidance Manual Alternative Disinfectants and
688 Oxidants. 1999. 3-10, NaN-3 p.
689 49. Sacco T. Personal communication. 2019.
690 50. Wu T, Englehardt JD. Peroxone mineralization of chemical oxygen demand for direct
691 potable water reuse: Kinetics and process control. Water Res [Internet]. 2015 Apr;73:362–72.
692 Available from: http://linkinghub.elsevier.com/retrieve/pii/S0043135415000585
693 51. Keen OS, McKay G, Mezyk SP, Linden KG, Rosario-Ortiz FL. Identifying the factors that
694 influence the reactivity of effluent organic matter with hydroxyl radicals. Water Res [Internet].
695 2014 Mar;50:408–19. Available from:
696 https://linkinghub.elsevier.com/retrieve/pii/S0043135413008555
697 52. Beltrán FJ, Encinar J, González JF. Industrial wastewater advanced oxidation. Part 2. Ozone
698 combined with hydrogen peroxide or UV radiation. Water Res [Internet]. 1997
699 Oct;31(10):2415–28. Available from:
700 http://linkinghub.elsevier.com/retrieve/pii/S004313549700078X
701 53. Thiruvenkatachari R, Vigneswaran S, Moon IS. A review on UV/TiO2 photocatalytic
702 oxidation process (Journal Review). Korean J Chem Eng. 2008;25(1):64–72.
703 54. von Gunten U, Hoigne J. Bromate formation during ozonization of bromide-containing
704 waters: Interaction of ozone and hydroxyl radical reactions. Environ Sci Technol [Internet].

705 1994 Jul;28(7):1234–42. Available from: http://pubs.acs.org/doi/abs/10.1021/es00056a009

706

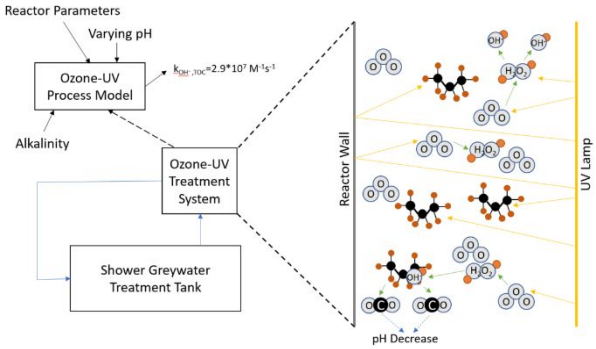

A novel ozone-UV kinetic model provides insight into ozone-UV organics mineralization, in particular varying organic load and pH during treatment.